PCCP

First-principles investigation of high capacity, rechargeable CF_x cathode batteries based on graphdiyne and "holey'' graphene carbon allotropes

Journal:	*Physical Chemistry Chemical Physics*
Manuscript ID	CP-ART-09-2024-003643.R1
Article Type:	Paper
Date Submitted by the Author:	15-Nov-2024
Complete List of Authors:	Campbell, Quinn; Sandia National Laboratories Paudel, Nirajan; New Mexico State University Acharya, Krishna; New Mexico State University Wygant, Bryan; Sandia National Laboratories, Department of Photovoltaics and Materials Technology Vasiliev, Igor; New Mexico State University, Physics Lambert, Timothy; Sandia National Laboratories, Materials, Devices & Energy Technologies

Journal Name

ARTICLE TYPE

Cite this: DOI: 00.0000/xxxxxxxxxx

First-principles investigation of high capacity, rechargeable CF_x cathode batteries based on graphdiyne and "holey" graphene carbon allotropes

Quinn T. Campbell,*[a] Nirajan Paudel,[b] Krishna Acharya,[b] Bryan R. Wygant,[c], Igor Vasiliev,[b] and T. N. Lambert[a]

Received Date
Accepted Date

DOI: 00.0000/xxxxxxxxxx

Batteries composed of CF_x cathodes have high theoretical specific capacities ($>$ 860 mAh/g). Attempts at realizing such batteries coupled with Li anodes have failed to deliver on this promise, however, due to a discharge voltage plateau below the theoretical maximum lowering the realized energy density and difficulties with recharging the system. In this study, we use first-principles calculations to investigate novel carbon allotropes for these battery systems: graphdiyne and "holey" graphene. We first identify stable flourination structures and calculate their band gaps. We demonstrate that the holes in these carbon allotropes can induce the formation of an amorphous LiF network within the carbon and that this formation may, in fact, be kinetically favored. For structures where amorphous LiF forms within the carbon, we predict it is easier to recharge and higher discharge voltages can be achieved. If the LiF forms outside the carbon product, however, it will be crystalline in form and lead to lower discharge voltages and more difficulty in recharging the systems. Finally, we simulate XPS spectra of representative cases, demonstrating an experimental pathway for determining the reaction pathway of these systems. Our work suggests CF_x allotropes with holes in them as potential targets for high capacitiy, rechargable cathodes for Li batteries, provided they lead to the formation of amorphous LiF within the C structure.

1 Introduction

Batteries made with fully flourinated CF_x cathodes exhibit a high theoretical specific capacity ($>$ 860 mAh/g)[1], and have been commercially developed as primary discharge batteries[2,3]. For coupling with a Li anode, these batteries undergo the following overall chemical reaction:

$$CF_x + xLi \rightarrow C + xLiF. \quad (1)$$

The carbon allotrope used in these reactions has typically been in the form of graphene, the idealized carbon basis for CF_x. For graphene allotropes, an average theoretical discharge value of $\approx$ 4.57 V has been reported[4,5].

Physical realizations of these systems using graphene as the carbon allotrope have much lower discharge values, typically plateauing around $\approx$ 2.5 V[6,7]. Leung *et al.* have explained this plateau by identifying an edge mediated mechanism, where Li comes into the "edge" of the graphene CF_x structure, pulling single F atom from the system and then subsequently removing to a LiF anode that forms outside the CF_x[5]. Furthermore, these systems generally are unable to recharge, unlike the chemically similar Na/CF_x system, although the exact nature of bond formation in these systems is still unclear[8,9]. Leung *et al.* attribute this to the difficulty of removing a F atom from crystalline LiF once formed[5]. Graphite and carbon nanotubes have also been studied as carbon precursors for CF_x systems, although none have totally overcome the issues mentioned above[10–12].

While the edge mediated mechanism provides a strong explanation for the mechanistic behavior of graphene CF_x batteries[13], the location of the LiF product remains a subject of some debate after discharge. Much work has also examined the possibility of Li intercalating between CF_x sheets[14,15], which would be similar to behavior seen in Na based CF batteries[16,17]. Furthermore, there seems to be some experimental evidence that in certain circumstance, LiF can end up forming an intermediate phase within the CF_x cathodes[18–21]. As a difficulty in recharging a graphene based CF_x electrode likely stems from the difficulty of pulling F off a crystalline LiF structure, it is reasonable to hypothesize that if one could encourage the formation of less crystalline LiF formation during discharge, recharge may be more facile.

*E-mail: qcampbe@sandia.gov
[a] *Center for Integrated Nanotechnologies, Sandia National Laboratories, Albuquerque, NM, USA*
[b] *Department of Physics, New Mexico State University, Las Cruces, NM, USA*
[c] Nanoscale Sciences Deparment, Sandia National Laboratories, Albuquerque, NM, USA

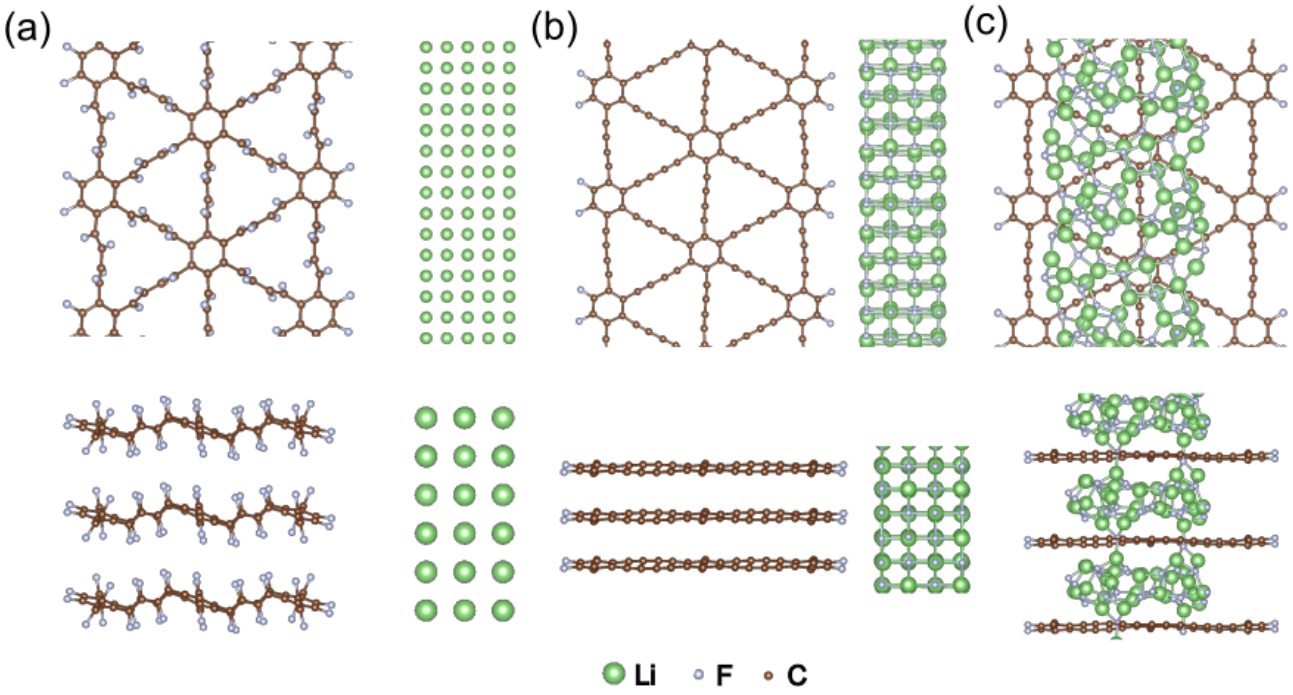

Fig. 1 The reaction pathway of CF_x electrodes could take two paths. Starting with (a) F terminated graphdiyne and a Li anode, the system could evolve to two configurations for the LiF: (b) crystalline LiF located outside of the C allotrope, or (c) amorphous LiF located within the graphdiyne allotrope layers, with LiF columns existing within the C holes.

In this work, we investigates if the use of alternative flourinated carbon allotropes could enable electrochemical recharge of Li/CF_x batteries. We use first-principles calculations to investigate two alternative carbon allotropes for CF_x based Li batteries: graphdiyne and "holey" graphene with a hole width of $\approx$ 12 Å. Both of these allotropes introduce holes within the larger CF_x structure. We first determine stable structures and flourinations for each of these structures as well as band gaps. As demonstrated in Fig. 1, we then examine two possible locations for LiF formation during discharge: crystalline formation outside the cathode, leading to an edge mediated discharge mechanism, and amorphous LiF formation between the C layers and extending through the holes in the graphdiyne of graphene. In the latter case, since removing F atoms from the C for these systems is not inherently edge mediated, we find higher possible discharge potentials ($\approx$3.5 V) can be achieved. Furthermore, recharging is also made easier for these amorphous LiF systems since F atoms do not have to break out of fully crystalline structures. Finally we demonstrate with XPS calculations that varying LiF structures should give distinct XPS signals, demonstrating an experimental pathway for determining the LiF formation mechanism in these systems. This work demonstrates that alternative carbon allotropes with significant holes in them may be a viable pathway for achieving higher theoretical discharge capacities promised by CF_x electrodes as well as enabling recharge– provided these carbon allotropes encourage the formation of intercalated amorphous LiF.

2 Methods

2.1 Computational Details

Electronic structure calculations are done using the Quantum ESPRESSO package[22]. We use norm-conserving pseudopotentials from the PseudoDojo repository[23] and the Perdew-Burke-Ernzerhof exchange-correlation functional[24]. We use kinetic energy cutoffs of 50 Ry and 400 Ry for the plane wave basis sets used to describe the Kohn-Sham orbitals and charge density, respectively. We use a $2\times2\times1$ Monkhorst-Pack grid[25] to sample the Brillioun zone in our calculations. Equilibrium structures are found by allowing the forces to relax below 0.05 eV/Å. We use the ENVIRON package[26] to calculate the parabolic corrections when running slab calculations. Reaction barriers were calculated using the Nudged Elastic Band method, as implemented within Quantum ESPRESSO.

Band structure calculations were carried out using ultrasoft Vanderbilt pseudopotentials[27] and kinetic energy cut offs of 60 Ry and 400 Ry for the plane wave basis set and charge density, respectively. An $8\times8\times1$ k-point grid was used for all GDY structures and a $4\times4\times1$ k-point grid was used for holey graphene. X-ray photoelectron spectra (XPS) were modeled by computing 1s core–electron binding energies of second-row elements using custom made all-electron projector augmented wave (PAW) pseudopotentials. The binding energies of core electrons were evaluated as the difference between the core electron ionization energy and the valence band maximum. The Brillouin zone was sampled using a $4\times4\times4$ k-point grid for the bulk LiF crystal and a $2\times2\times1$ k-point grid for the LiF monolayer and amorphous LiF. The LiF

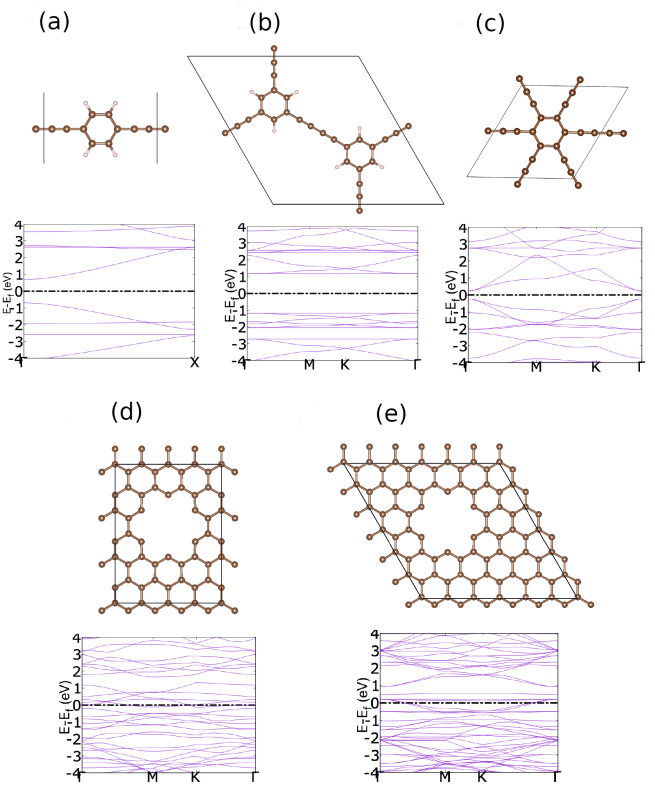

Fig. 2 Optimized geometries and calculated band structures of (a) 1,4-GDY, (b) 1,3,5-GDY, (c) γ-GDY, and holey graphene in (d) rectangular and (e) hexagonal cells.

monolayer was constructed by adding a vacuum layer to the periodic cell. The XPS spectra of Li_nF_n clusters were calculated at the Gamma point by placing the cluster inside a cubic box with an edge of 20 Å.

3 Results

3.1 Structures and Electronic Properties of Carbon Allotropes

Low-dimensional carbon allotropes with sp and sp^2 hybridization are regarded as promising electrode materials for batteries[28,29]. To identify the potentially better performing CF_x cathode materials, we examined the structures and electronic properties of several low-dimensional carbon allotropes, including a linear graphdiyne chain (1,4-GDY)[30], a planar 1,3,5-graphdiyne (1,3,5-GDY), gamma-graphdiyne (γ-GDY)[31], and a holey graphene[32]. Optimized geometries and calculated electronic band structures of these carbon allotropes are shown in Fig. 2. To analyze the influence of supercell symmetry on the electronic properties of holey graphene, its atomic structure was modeled using both rectangular and hexagonal supercells.

The calculated band structures of 1,4-GDY, 1,3,5-GDY, and γ-GDY showed that these carbon allotropes were semiconducting and had nonzero band gaps. Our calculations predicted direct band gaps of 1.41 eV for 1,4-GDY, 2.37 eV for 1,3,5-GDY, and 0.47 eV for γ-GDY, respectively. In contrast, holey graphene was found to be a conducting material with zero band gap in both rectangular and hexagonal supercells.

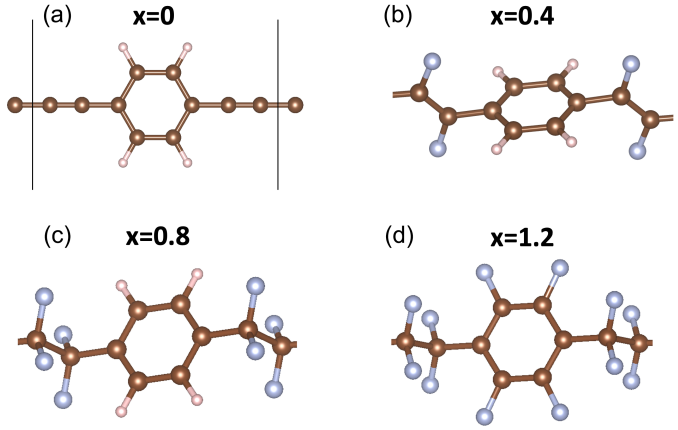

Fig. 3 Step-by-step mechanism of fluorination of 1,4-GDY. The fluorination process is shown at (a) $X = 0$, (b) $X = 0.4$, (c) $X = 0.8$, and (d) $X = 1.2$, where X is the fluorine content in CF_x.

3.2 Fluorination of Carbon Allotropes

In the next step, we investigated the sequential fluorination of carbon allotropes with the formula CF_x. Figure 3 illustrates a step-by-step fluorination process of 1,4-GDY. Fluorination of 1,4-GDY was carried out in three stages. During the first stage, $0 < X \leq 0.4$, fluorine atoms were attached to the triple C≡C bonds of 1,4-GDY. The resulting F-C bonds were orthogonal to the plane of the benzene ring and alternated between up and down positions. During the second stage, $0.4 < X \leq 0.8$, second fluorine atoms were attached to the same carbon atoms, changing their hybridization from sp^2 to sp^3. The equilibrium angle between the F-C-F bonds was close to 108°. During the third stage, $0.8 < X \leq 1.2$, hydrogen atoms on the benzene ring were replaced with fluorine atoms. The resulting F-C bonds were parallel to the benzene ring. The electronic band gaps of fluorinated 1,4-GDY increased with the increasing level of fluorination from 1.41 eV for $X = 0$ to 3.33 eV for $X = 1.2$.

The sequential fluorination of 1,3,5-GDY is shown in Fig. 4. Fluorination of 1,3,5-GDY was performed in three stages. During the first two stages, $0 < X \leq 1/6$ and $1/6 < X \leq 0.5$, fluorine atoms were attached to the different C≡C bonds of 1,3,5-GDY. The resulting F-C bonds were parallel to the plane of the benzene ring. During the third stage, $0.5 < X \leq 0.75$, hydrogen atoms on the benzene ring were replaced with fluorine atoms. The resulting F-C bonds were also parallel to the benzene ring. We found that fluorination above the $X = 0.75$ level resulted in structural distortion and instability of fluorinated 1,3,5-GDY.

Figure 5 illustrates the fluorination process of γ-GDY. Fluorination of γ-GDY was carried out in two stages. During the first stage, $0 < X \leq 2/3$, fluorine atoms were attached to the C≡C bonds of γ-GDY. The created F-C bonds were orthogonal to the benzene ring and alternated between up and down positions. During the second stage, $2/3 < X \leq 4/3$, second fluorine atoms were attached to the same carbon atoms. Our calculations showed that the electronic band gaps of fluorinated γ-GDY increased from 0.47 eV for

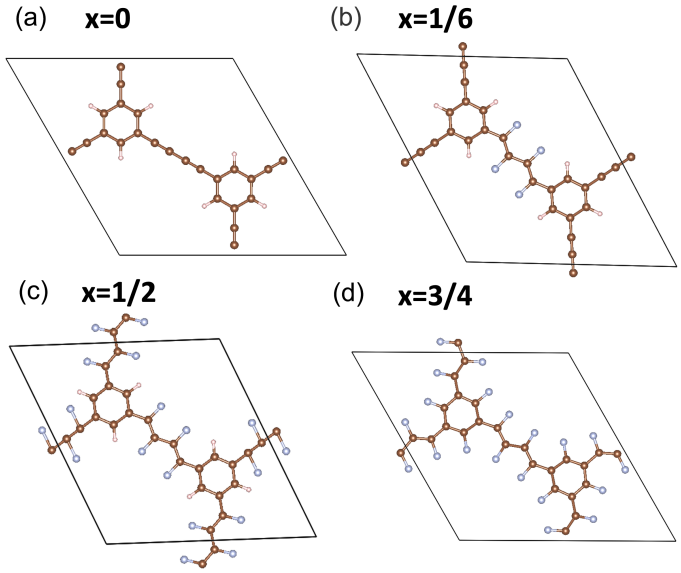

Fig. 4 Step-by-step fluorination of 1,3,5-GDY. The fluorination process is shown at (a) $X = 0$, (b) $X = 1/6$, (c) $X = 0.1/2$, and (d) $X = 3/4$. X is the fluorine content in CF_x.

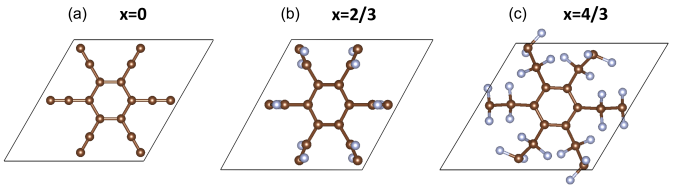

Fig. 5 Step-by-step fluorination of γ-GDY. The fluorination process is shown at (a) $X = 0$, (b) $X = 2/3$, and (c) $X = 4/3$. X is the fluorine content in CF_x.

$X = 0$ to 1.38 eV for $X = 2/3$ and 3.57 eV for $X = 4/3$.

The sequential fluorination of holey graphene is displayed in Fig. 6. For this study, we selected the rectangular holey graphene supercell shown in Fig. 2(d). Fluorination of holey graphene was performed in two steps. During the first step, $0 < X \leq 1/7$, fluorine atoms were attached to the carbon atoms at the edges of the hole. The resulting F-C bonds were parallel to the plane of graphene. During the second step, $1/7 < X \leq 8/7$, the surface of graphene was fluorinated. The resulting F-C bonds were orthogonal to the graphene plane and the attached fluorine atoms alternated between up and down positions. The calculated electronic band gap increased from 0 eV for non-fluorinated holey graphene to 3.59 eV for fully fluorinated holey graphene.

Calculated fluorination energies of 1,4-GDY, 1,3,5-GDY, γ-GDY, and holey graphene are compared in Fig. 7. The fluorination energies per fluorine atom were calculated using Eq. (2) for fluorine atoms attaching to the carbon chains and Eq. (3) for fluorine atoms replacing hydrogen atoms on the benzene rings.

$$\Delta E_F = \frac{1}{N}\left(E_r - E_i - \frac{N}{2}E_{F_2}\right), \quad (2)$$

$$\Delta E_F = \frac{1}{N}\left(E_r - E_i - NE_{F_2} + NE_{HF}\right), \quad (3)$$

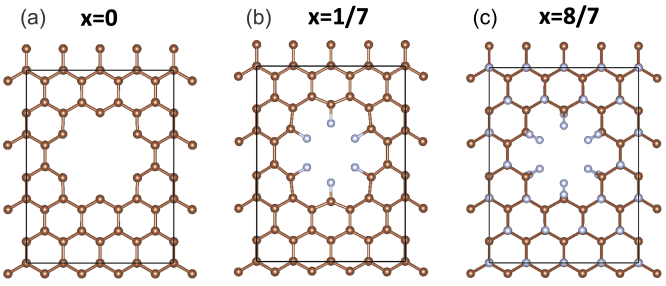

Fig. 6 Fluorination of holey graphene. The fluorination process is shown at $X = 0$, (b) $X = 1/7$, and (c) $X = 8/7$. X is the fluorine content in CF_x.

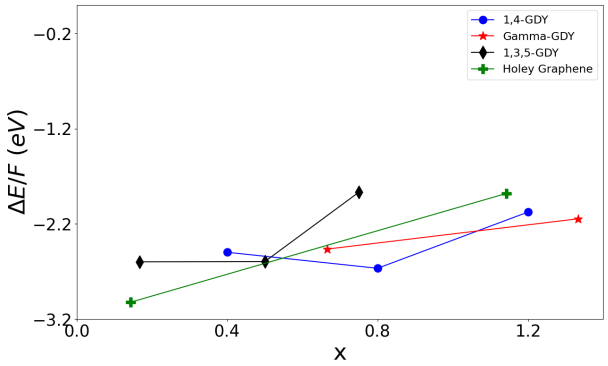

Fig. 7 Calculated fluorination energies of 1,4-GDY, 1,3,5-GDY, γ-GDY, and holey graphene. The energies are given in eV per F atom. X is the fluorine content in CF_x.

where E_i and E_r were the total energies of the system before and after fluorination, E_{F_2} and E_{HF} were the energies of F_2 and HF molecules, and N was the number of attached fluorine atoms. Our calculations showed that for $X \leq 0.75$, the fluorination energies of the three studied graphdiynes were close to each other and appeared to be almost independent of the fluorine content. In the range of $X \geq 0.75$, the energies of fluorination for 1,4-GDY, 1,3,5-GDY, and γ-GDY, slightly increased with the with the increasing level of fluorination from about -2.5 eV to about -2.0 eV. The fluorination energy of holey graphene during the first stage of fluorination, $0 < X \leq 1/7$, was found to be approximately 0.5 eV lower than that for the studied graphdiynes. However, in the range of $1/7 < X \leq 8/7$, the energy of fluorination of holey graphene was close to that for 1,4-GDY, 1,3,5-GDY, and γ-GDY.

The computed fluorination energies of 1,4-GDY, 1,3,5-GDY, γ-GDY, and holey graphene were applied to estimate the equilibrium Li/CF_x defluorination voltage for these carbon allotropes. The computed formation energy of solid LiF was found to be $\Delta E_{LiF} = -5.9$ eV per atomic pair using a DFT computational method combined with the GGA-PBE exchange-correlation functional. This was calculated as the difference between the total energies of solid LiF, solid Li and F_2 (gas): Li(s) + $\frac{1}{2}F_2$(g) –> LiF(s). This value was about 10% lower than the experimental formation enthalpy of LiF. The equilibrium Li/CF_x defluorination

Table 1 Calculated fluorination energies and equilibrium defluorination voltages for 1,4-GDY, 1,3,5-GDY, γ-GDY, and holey graphene.

Structure	X	ΔE_F (eV)	V_i (V)
1,4-GDY			
	0.4	-2.50	3.40
	0.8	-2.67	3.23
	1.2	-2.08	3.82
1,3,5-GDY			
	1/6	-2.60	3.30
	1/2	-2.60	3.30
	3/4	-1.87	4.03
γ-GDY			
	2/3	-2.46	3.44
	4/3	-2.15	3.75
holey graphene			
	1/7	-3.02	2.88
	8/7	-1.88	4.02

voltage was evaluated as

$$V_i = \Delta E_F - \Delta E_{LiF}, \tag{4}$$

where the voltage V_i was in volts and the energies ΔE_F and ΔE_{LiF} were in eV per fluorine atom. The computed defluorination voltages for 1,4-GDY, 1,3,5-GDY, γ-GDY, and holey graphene in the range of $0 < X \leq 4/3$ are summarized in Table 1.

According to our calculations, the equilibrium defluorination voltages for 1,4-GDY, 1,3,5-GDY, and γ-GDY in the range of $0 < X \leq 0.5$ were predicted to be around 3.3-3.4 V. The equilibrium defluorination voltage for holey graphene at low fluorination level was estimated to be around 2.9 V. At a higher fluorination level, $X \geq 0.5$, the equilibrium defluorination voltages for 1,4-GDY, 1,3,5-GDY, γ-GDY, and holey graphene were found to be in the range of 3.8-4.0 V.

3.3 LiF product formation

As shown in Fig. 1 for γ-graphdiyne with $X = 2/3$, we examine two different mechanisms for LiF formation upon discharge: (1) crystalline LiF formation outside of a layered C cathode, and (2) amorphous LiF formation within the C cathode. We suggest that the latter outcome is particularly likely in these C allotropes, as the holes within the graphdiyne and graphene allow extra channels for amorphous LiF columns to form within the cathode. Nevertheless it is important to examine the thermodynamic stability of each option.

For graphdiyne, we see that externally realized crystalline LiF formation is the most thermodynamically favorable, as expected, with a formation energy of -0.5 eV/LiF compared to a single layer crystalline structure with the same number of atoms, where the formation energy is calculated as

$$\Delta E_F = (E_{\text{crystal}} - E_{\text{layer}})/n_{\text{LiF}}, \tag{5}$$

where E are DFT calculated energies and n_{LiF} is the number of LiF units within the structure. Amorphous LiF formation, however, is also thermodynamically favorable compared to the crystalline layered structure with a formation energy of -0.19 eV/LiF. This less favorable energy can be attributed to the amorphous structures less maximally satisfying Li-F bonds, due to the interaction with the underlying CF_x. Nonetheless, these results indicate that both LiF products can be achieved with thermodynamic stability, depending on the specific mechanism involved in discharging the system.

We see a similar story in holey graphene, as shown in Fig. 8. We model two different processes for the broad chemical reaction Eq. 1: (1) crystalline LiF formation outside of the layered graphene structure, and (2) amorphous LiF formation within the hole of the holey graphene. We again see that the crystalline LiF outside of the graphene is slightly more thermodynamically favorable, with a formation energy of -0.56 eV/LiF atom compared to a layered crystalline LiF layer. The amorphous LiF is still favorable, however, with a formation energy of -0.34 eV/LiF. Both structures are again favorable and the final outcome will therefore be dependent on the kinetics of the exact reaction pathways taking place. We have not modeled solvent effects due to the computational complexity, but we note that here they are likely to play a significant role in directing which phase of LiF stabilizes most readily in a given system. Note that the hole simulated for our holey graphene is only $\approx$ 12 Å wide. This implies that even relatively small holes can lead to stable amorphous LiF formations.

For the amorphous LiF structures within both the graphdiyne and holey graphene, we performed phonon calculations around the Γ point and found no imaginary frequencies for the vibrational modes. This further demonstrates the stability of these structures. See the supporting information for more details on these phonon calculations. While it is not possible to determine that these are global minimum atomic structures, we have investigated a number of alternatives and are displaying the lowest energy structures after geometry optimization. The structures of similar, but higher energy, structures that we tested can also be found in the supporting information.

3.4 Kinetics of LiF formation

While crystalline LiF is thermodynamically most favorable, kinetics will ultimately decide whether LiF is most likely to form as an amorphous mixture within the graphdiyne or as an external crystalline material. While it is ultimately out of scope for us to simulate the entire reaction pathway, we have simulated the reaction barriers for the initial atom migrations in these systems. In Fig. 9, we demonstrate two initial reaction paths for LiF formation. We start with an F terminated graphdiyne cathode near a metallic Li anode, and then measure the reaction barrier for either a Li migrating from the Li anode toward the CF_x cathode or a F migrating from the CF_x cathode to the Li anode. We find that the reaction barrier for Li migrating toward the cathode is 0.61 eV, while the reaction barrier for F migrating toward the Li anode is 3.28 eV. These results imply that it is significantly easier to nudge the system toward Li moving into the graphdiyne, seeding the beginning of an amorphous LiF mixture. Due to computational restrictions, we do not include any solvent effects in this calculation, which could significantly change the reaction barriers shown here. These calculations should be thought of as a useful

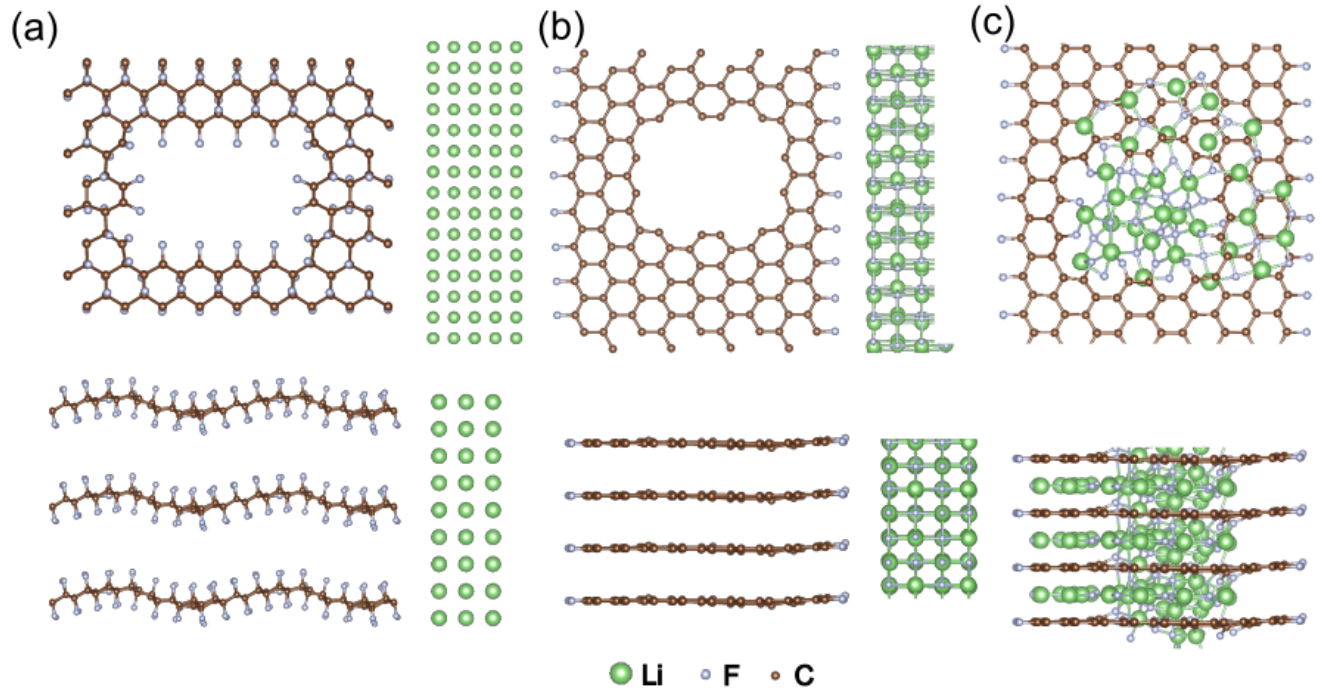

Fig. 8 Starting with (a) F terminated holey graphene and a Li anode, the system could evolve to two configurations for the LiF: (b) crystalline LiF located outside of the C allotrope, or (c) amorphous LiF located within the holey graphene layers, with LiF columns existing within the C holes.

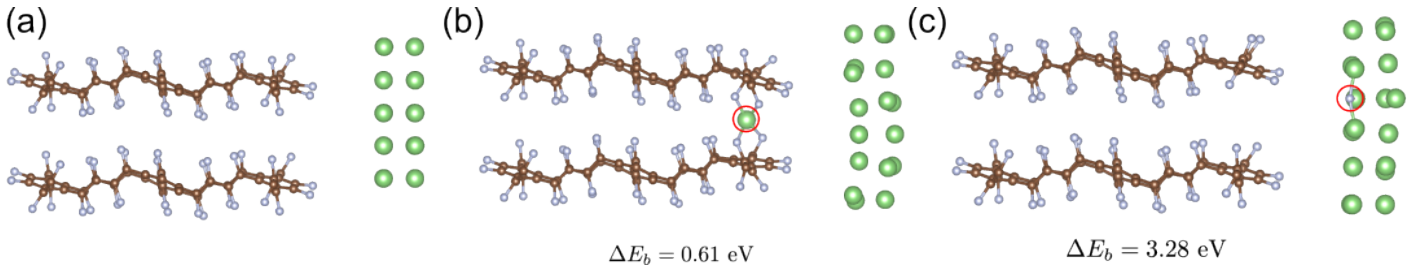

Fig. 9 Initial kinetics of LiF formation. Starting from (a) a F terminated graphdiyne cathode next to a Li anode, we caclulate the reaction barrier of either (b) a Li atom migrating from the anode to bond with the CF_x structure, beginning the formation of an amorphous LiF network, or (c) a F atom migrating from the CF_x cathode toward the nearby Li anode, forming

first approximation at the kinetics of such a system.

Thus the amorphous LiF structure may, in fact, be kinetically favored, making its properties for discharge and recharge worthy of investigation.

3.5 Discharging

The equilibrium discharge potential $\mathscr{V}_{\text{crystalline}}$ associated with an incremental movement δx of Li into the CF_x structure that then goes on to form crystalline LiF

$$CF_x + \delta x\text{Li} \rightarrow CF_{x-\delta x} + \delta x\text{LiF} \tag{6}$$

can be measured as

$$e\mathscr{V}_{\text{crystalline}} = -\left[E(CF_x) - E(CF_{x-\delta x})\right]/\delta x + E(\text{LiF}) - E(\text{Li}), \tag{7}$$

where E represents the DFT calculated energy of each respective component. This equation assumes that the resulting LiF product is forming in a crystalline manner, however. For incremental defluorination where the LiF forms amorphous structures within the CF_x allotropes, we can determine the discharge voltage $\mathscr{V}_{\text{amorphous}}$ from the chemical reaction

$$CF_x + \delta x\text{Li} \rightarrow CF_x\text{Li}_{\delta x}, \tag{8}$$

which gives

$$e\mathscr{V}_{\text{amorphous}} = -\left[E(CF_x) - E(CF_x\text{Li}_{\delta x})\right]/\delta x - E(\text{Li}). \tag{9}$$

In the case of graphdiyne, we find a discharge voltage for crystalline LiF of $\mathscr{V}_{\text{crystalline}} = 1.46$ V, assuming that the system follows the edge mediated mechanism put forward by Leung *et al.*[5]. This is significantly lower than the ≈2.5 V discharge potential found for graphene, indicating that graphdiyne may actually be disadvantageous as a battery material with an edge mediated mechanism.

For the formation of amorphous LiF within the graphdiyne cathode, the reaction mechanism can proceed along several paths

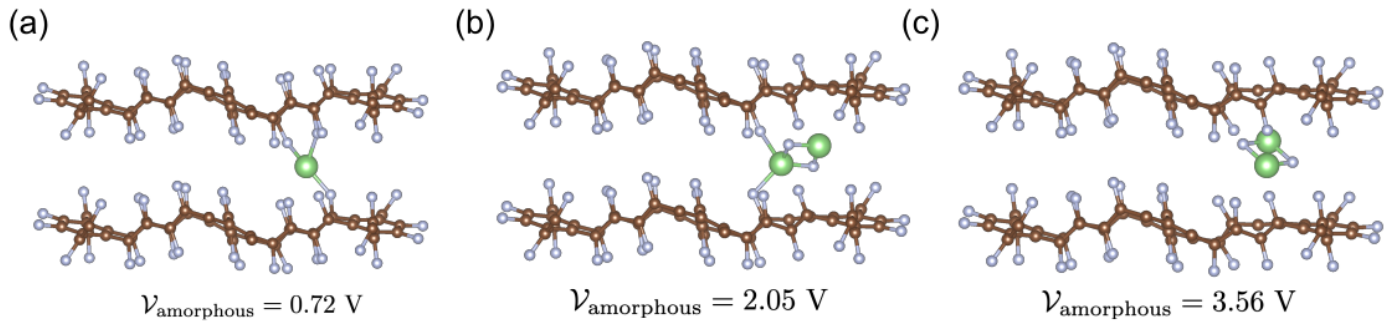

Fig. 10 Different configurations of initial amorphous LiF formation within graphdiyne: (a) a single Li is introduced, attached to several F atoms, (b) a LiF square forms, while still being significantly connected to the CF_x structure, and (c) formation of a LiF square which detatches from the CF_xj strucutre into the hole within the C allotrope.

with Li intercalating within the cathode to form LiF fragments. As shown in the supporting information, the Li does not attach to C atoms on their own and will typically migrate toward the F atoms due to their electrostatic attraction. These LiF fragments then remain caught within the broader CF_x framework, forming the seed for further amorphous LiF growth. We test a variety of configurations for the initial Li atom insertion and formation, with representative examples shown in Fig. 10. The calculated discharge voltage varies significantly depending on the location and nature of Li insertion. When a Li atom is initially intercalating into the CF_x structure, it tends to bond with multiple F atoms and have a lowered discharge voltage of ≈0.7 - 0.8 V, with a typical example shown in Fig. 10a. When a LiF fragment begins to form within the graphdiyne structure, but still has connection to the underlying graphdiyne, we find discharge voltages of ≈ 2 V, with a typical example shown in Fig. 10b. Finally, when amorphous LiF begins to form within the holes of the graphdiyne, pulling away from the carbon, the discharge voltage can approach ≈3.5 V, with a representative example shown in Fig. 10c. While our exploration of LiF formation was nowhere near exhaustive, these three possibilities seem to be broadly matched within our calculations.

This presents two possible discharge voltage profiles for the formation of amorphous LiF. In the first, three distinct plateaus are seen, with heights of ≈0.75 V, 2 V, and 3.5 V. This route implies that one of these mechanisms would dominate for significant portions of LiF formation and then be replaced by another mechanism. For instance, these voltages could correspond to separate stages of nucleation and growth of the LiF within the CF_x structure, as the predicted discharge voltage in our calculations tends to increase as the LiF formation grows. If the higher voltage mechanisms at 3.5 V dominate for a significant portion of time, this could lead to enhanced energy density compared to graphene based cathodes. Another possibility is that this would experimentally realized as a sloping discharge profile, with the energy density benefits dependent on the relative amount of time spent above 2.5 V. This discharge would likely still be distinguishable from the edge mediated formation of crystalline LiF, which has a discharge potential of ≈ 1.5 V and would likely show as a voltage plateau experimentally. Discharge potentials could thus be used to help distinguish the LiF phase formation mechanism within the system.

The discharge pathway in holey graphene looks quite similar. We assume that if discharge follows the edge mediated mechanism to form crystalline LiF, the voltage will match the previous graphene edge calculations (of ≈ 2.5 V), as the hole would be perpendicular to the fundamental mechanisms geometry and thus have little impact.

For amorphous LiF formation, a number of reaction mechanisms are again possible. The discharge voltage distribution again has three broad peaks, with case examples shown in Fig. 11. The pattern of low to high discharge voltages switches in these examples, although voltages in all three cases are higher than in graphdiyne. In systems where LiF forms and then inserts itself into the graphene holes, the discharge voltage is typically lower, ≈0.85 V, as shown in Fig. 11a. When the LiF is partially connected to the underlying graphene structure, the voltage tends to rise to ≈2.6 V, as shown in Fig. 11b. Finally, when the LiF is significantly bonded with the underlying CF_x, the voltage can reach ≈ 4 V, as shown in Fig. 11c. This again leads to two possible discharge paths. One where there are three distinct voltage plateaus and a potentially significant increase in overall specific capacity. In the other possibility, we would likely see a sloped discharge profile as the system evolves through these different phases. The fact that both of the graphdiyne system and the holey graphene system see increasing voltage as the LiF grows indicates that this may be a nucleation effect, with the higher discharge voltages reached relatively early in the lithiation. Both of these paths likely deviate from the discharge voltage plateau at ≈ 2.5 V that we would see if LiF formation takes place via the edge mechanism. Once again, experimental measures of discharge can be useful in distinguishing between these possibilities.

3.6 Recharging

While the discharge profiles of amorphous LiF formation in graphdiyne and holey graphene present potential but uncertain improvement over edge mediated crystalline LiF formation, the ability of the system to recharge is significantly improved. For an edge mediated mechanism, we calculate the thermodynamic energy difference ΔE of F migration away from the LiF to the

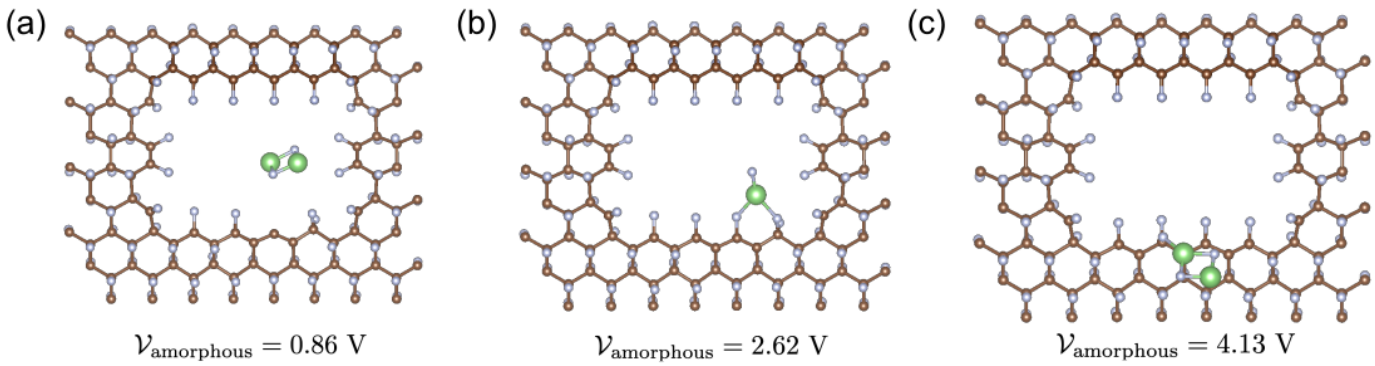

Fig. 11 Different configurations of initial amorphous LiF formation within holey graphene: (a) formation of a LiF square detatched from the system, (b) initial introduction of a Li atom which pulls of neighboring F, and (c) formation of a LiF square which is squeezed between the CF_x layers.

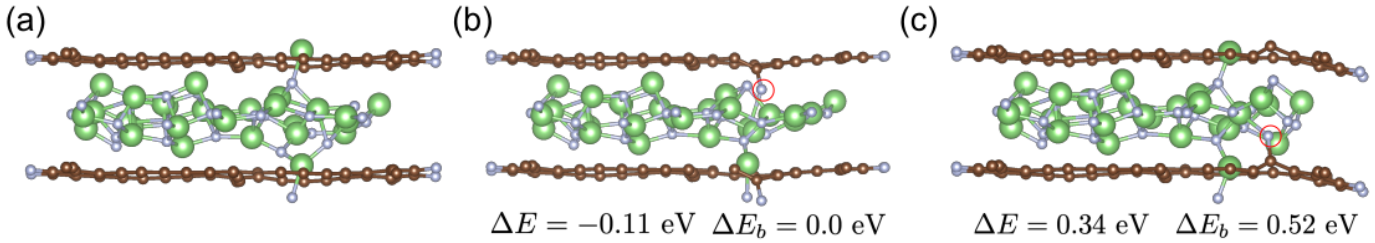

Fig. 12 Initial recharge pathways for graphdiyne. (a) A final amorphous LiF structure incorporated within graphdiyne layers and holes. (b) An initial migration of F away from the LiF onto a C atom. (c) A second F atom's migration from the LiF to the graphdiyne C.

graphdiyne edge as measured by

$$\Delta E = E(\mathrm{CF}_{x+\delta x} + \mathrm{LiF}_{1-\delta x}) - E(\mathrm{CF}_x + \mathrm{LiF}) \tag{10}$$

to be 1.65 eV. In this convention, positive ΔE represent unfavorable outcomes. This is a relatively high energetic cost, and is compounded by an even higher kinetic reaction barrier, $\Delta E_b = 2.3$ eV. This means that significant energy would have to be put into the graphdiyne system to make recharge favorable, due to the difficulty of breaking the crystalline LiF bonds.

In amorphous LiF systems, however, the energy needed to break LiF bonds is significantly less. We simulate the thermodynamic energy difference and energy barrier of the first F atoms moving away from LiF toward graphdiyne C atoms in Fig. 12. For the first F atom migration we find an effortless recharge process, with a thermodynamically favorable $\Delta E = -0.11$ eV and no reaction barrier. For the second F atom migration we do see an energy requirement with a $\Delta E = 0.34$ eV and a reaction barrier of $\Delta E_b = 0.52$ eV. These energies are significantly smaller than the energies needed for recharge in a crystalline LiF system, and may be achievable at reasonable temperature/voltage conditions. The lowered energy requirements of recharge from an amorphous LiF system can be attributed to the lower cohesive energy of the amorphous LiF, making it easier to break bonds, as well as convenient to migrate to nearby carbons.

Amorphous LiF formation in holey graphene likewise provides an opportunity for significantly lowering energy requirements for recharge of the battery. For an edge mediated crystalline LiF formation mechanism we can again assume the thermodynamic value from Leung *et al.*'s previous study: $\Delta E = 2.44$ eV[5]. We then investigate the energy costs of F migration from amorphous LiF onto the holey graphene C atoms in Fig. 13. We find the first F atom migrates with an energetic cost of $\Delta E = 0.64$ eV and a kinetic barrier of $\Delta E_b = 0.68$ eV. The second F atom migration has an energetic cost of $\Delta E = 0.37$ eV and a kinetic barrier of $\Delta E_b = 0.39$ eV. These lower energy costs can directly be attributed to the easier nature of breaking amorphous LiF bonds.

These lowered energy requirements raise the possibility of CF_x batteries paired with Li anodes that exhibit the ability to recharge, greatly expanding possible use cases and economics of CF_x development. The consistency of the results within simulations of both graphdiyne and holey graphene indicates that the key feature for lowered recharge energy requirements is the formation of amorphous LiF. This can likely be achieved in many CF_x systems with similar holes throughout the structure, allowing for flexibility of battery preparation. This outcome presents new possible synthetic targets to experimentally verify our findings.

3.7 Simulated XPS Spectra

We have proposed alternative reaction mechanisms for LiF formation with carbon allotropes that may lead to improved battery performance. It would be ideal, however, if we could experimentally verify the proposed mechanism when examining these battery chemistries. X-ray photoelectron spectroscopy (XPS) is an experimental technique commonly used for elemental analysis and surface characterization of organic and inorganic materials[33]. Because XPS is highly sensitive to the elemental chemical state and

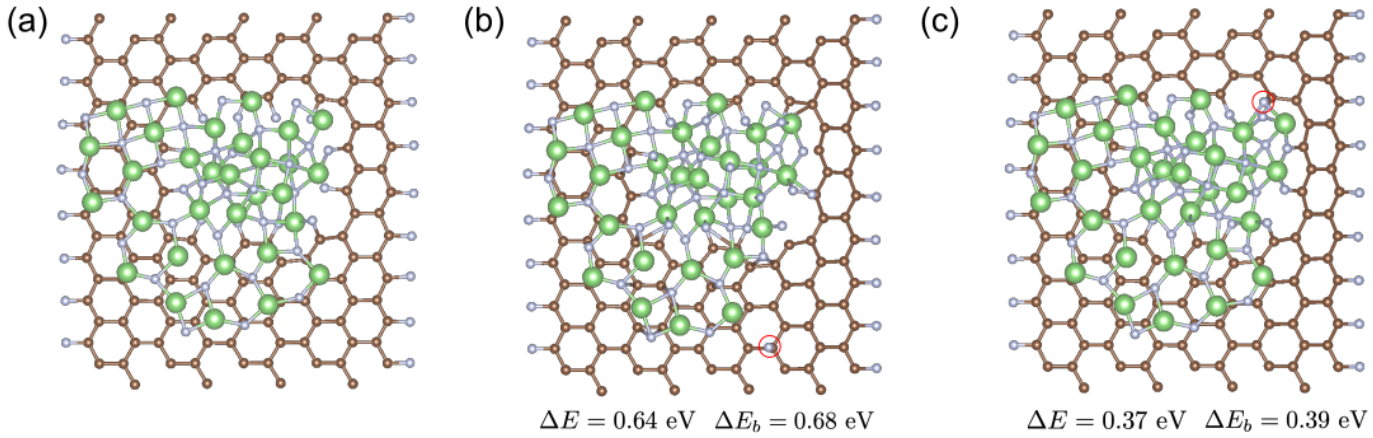

Fig. 13 Initial recharge pathways for holey graphene. (a) A final amorphous LiF structure incorporated within holey graphene layers and holes. (b) An initial migration of F away from the LiF onto a C atom. (c) A second F atom's migration from the LiF to the holey graphene C.

surface composition of the studied materials, it could help identify the morphology and distribution of LiF in Li/CF_x batteries. To demonstrate the feasibility of this approach, we compared simulated XPS spectra of different LiF structures, including crystalline LiF, amorphous LiF, LiF monolayer, and small LiF clusters. Theoretical XPS spectra were modeled by computing the binding energies of core electrons for the F 1s level and applying a Gaussian broadening of 0.005 Ry. The core electron binding energies were evaluated as the difference between the core electron ionization energy and the valence band maximum (VBM)[34]. To improve agreement with the experimental XPS spectra, simulated XPS peaks were shifted by the difference between the calculated and experimental values of the core electron binding energy for the F 1s level in a bulk LiF crystal[35].

The calculated structures of a LiF crystal, amorphous LiF, LiF monolayer, and several small Li_nF_n clusters in the size range $n = 2-16$ are shown in Fig. 14. The computed XPS spectra of the F 1s core level for these structures are presented in Fig. 15. The initial atomic configurations of Li_nF_n clusters were adapted from Doll *et al.*[36] and Yin *et al.*[37]. The final cluster geometries were obtained via structural optimization. The atomic structure of amorphous LiF used in our XPS calculations was adapted from Fig. 12(a). The equilibrium structure of a LiF monolayer was obtained by adding a vacuum layer to the periodic cell and performing a variable-cell optimization, during which the lattice vectors parallel to the surface of the monolayer were allowed to relax, but the lattice vector orthogonal to the surface was kept constant.

The calculated binding energies of the F 1s core electrons in a bulk LiF crystal, LiF monolayer, amorphous LiF, and small Li_nF_n clusters are compared in Fig. 16. For the LiF structures with multiple XPS peaks, the plot shows the weighted average value of the core electron binding energy. We observed significant differences in the positions of simulated XPS spectral lines for the crystalline, amorphous, and monolayer forms of LiF. Our calculations predicted the average F 1s core electron binding energies of 684.4 eV for the LiF monolayer, 684.8 eV for the amorphous LiF, and 685.0 eV for the LiF crystal. The absolute values of the F 1s core electron binding energies for small Li_nF_n clusters increased with

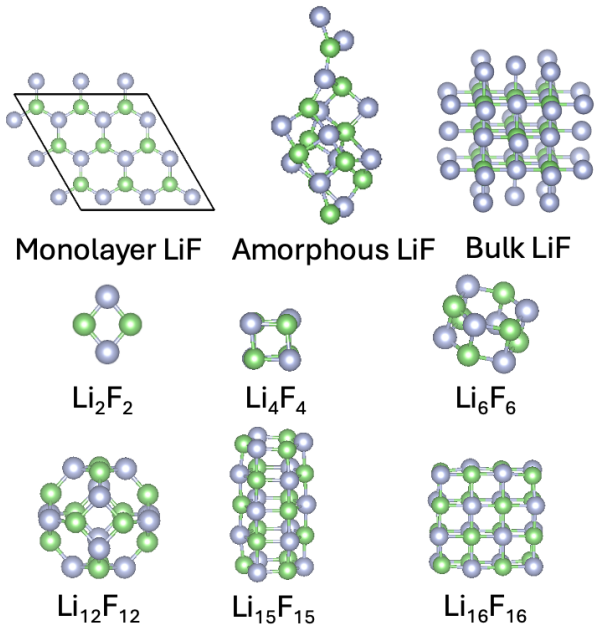

Fig. 14 Calculated structures of a LiF monolayer, amorphous LiF, a bulk LiF crystal and small Li_nF_n clusters.

increasing the size of the cluster. The simulated XPS spectra of Li_nF_n clusters in the size range $n = 2-12$ were found to be similar to the XPS spectrum of the LiF monolayer. In contrast, the XPS spectra of larger LiF clusters appeared to be closer to those of the amorphous and crystalline LiF. This result was consistent with the emergence of semi-amorphous and bulk-like structures for the Li_nF_n clusters in the size range $n = 15-16$. Overall, our study indicated a relatively straightforward relationship between the size of the F 1s XPS chemical shift and the effective average coordination number of Li ions in LiF structures. The results of our calculations suggest the possibility of using XPS for determining the structural and morphological properties of LiF in Li/CF_x batteries.

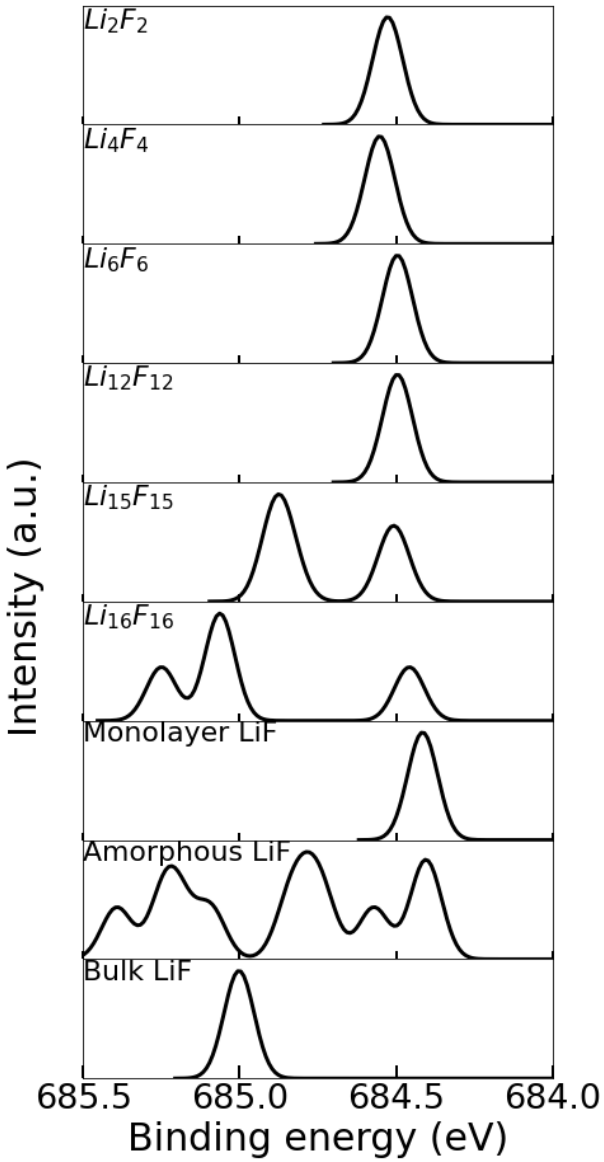

Fig. 15 Simulated F 1s X-ray photoelectron spectra (XPS) of small Li_nF_n clusters, a LiF monolayer, amorphous LiF, and a bulk LiF crystal. A Gaussian broadening of 0.005 Ry ($\sim$ 0.08 eV) was applied to the calculated XPS spectra.

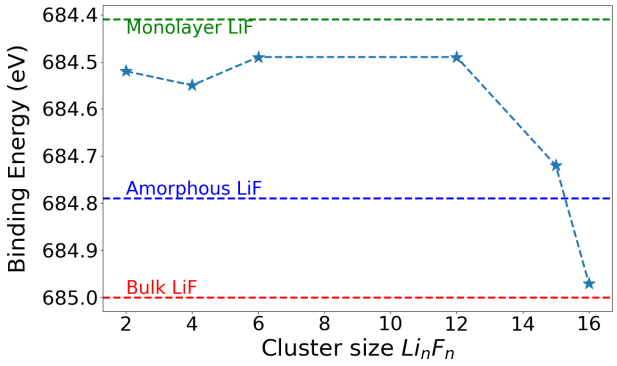

Fig. 16 Calculated average binding energies of core electrons for the F 1s level in a bulk LiF crystal, LiF monolayer, amorphous LiF, and small Li_nF_n clusters.

4 Conclusion

CF_x batteries with Li anodes have a high theoretical specific capacity, but have limited applications due to their lower real world discharge voltage and inabilitiy to recharge, limiting their applications to primary batteries. Practical and theoretical work on these systems have largely focused on CF_x in the form of flourinated graphene or graphene-like carbons. In this work, we explore the alternative carbon allotropes of graphdiyne and holey graphene as cathodes in the CF_x-Li battery system. We first find the stable flourination structures of these systems as a function of the total number of F added. We then explore how these systems may react to discharge and recharge reactions. We find that the holes within the graphdiyne and holey graphene structures induce another stable phase of LiF, where the LiF forms an amorphous structure layered between the graphdiyne/holey graphene layers and through the holes in the structure. We demonstrate that the formation of amorphous LiF may be kinetically favored with a lower reaction barrier for the first atom's movement. If such an amorphous LiF structure were to form, it would likely have a sloping discharge profile with magnitudes of up to $\approx$ 4.0 V. If the higher discharge voltages were to dominate,this may lead to increased energy density compared to graphene based CF_x systems. Furthermore, recharge becomes significantly easier to achieve both thermodynamically and kinetically for the amorphous LiF system as the energy of bond breaking is less than if crystalline LiF is formed. We also predict XPS spectra for a variety of LiF structures, showing that this may be a useful experimental route for distinguishing between the reaction pathways identified in this work.

These outcomes present a new heuristic for possible synthetic targets for Li/CF_x batteries. Our work suggests that C allotropes with significant holes within layers, such as graphdiyne and holey graphene, may make excellent cathode targets for high specific capacity, rechargable Li/CF_x based batteries. These enhanced qualities are dependent, however, on holes within the carbon structure inducing the formation of amorphous LiF layers intermixed with the CF_x cathode. Further theoretical and experimental work is needed to determine the exact reaction pathways of

LiF formation in these structures and how they interact with different CF_x allotropes.

Acknowledgments

We would like to thank Kevin Leung for useful discussions on the direction of the work.

This work was supported by the Laboratory Directed Research and Development program at Sandia National Laboratories under project 229404. This work was performed, in part, at the Center for Integrated Nanotechnologies, an Office of Science User Facility operated for the U.S. Department of Energy (DOE) Office of Science.

Sandia National Laboratories is a multi-mission laboratory managed and operated by National Technology & Engineering Solutions of Sandia, LLC (NTESS), a wholly owned subsidiary of Honeywell International Inc., for the U.S. Department of Energy's National Nuclear Security Administration (DOE/NNSA) under contract DE-NA0003525. This written work is authored by an employee of NTESS. The employee, not NTESS, owns the right, title and interest in and to the written work and is responsible for its contents. Any subjective views or opinions that might be expressed in the written work do not necessarily represent the views of the U.S. Government. The publisher acknowledges that the U.S. Government retains a non-exclusive, paid-up, irrevocable, world-wide license to publish or reproduce the published form of this written work or allow others to do so, for U.S. Government purposes. The DOE will provide public access to results of federally sponsored research in accordance with the DOE Public Access Plan.

Notes and references

1 J. L. Wood, A. J. Valerga, R. B. Badachhape and J. L. Margrave, *National Technical Information Service*, 1972, **755**, 934.

2 G. G. Amatucci and N. Pereira, *Journal of Fluorine Chemistry*, 2007, **128**, 243–262.

3 Q. Zhang, K. J. Takeuchi, E. S. Takeuchi and A. C. Marschilok, *Physical Chemistry Chemical Physics*, 2015, **17**, 22504–22518.

4 R. Fan, B. Yang, Z. Li, D. Ma, W. Yuan, J. Ma and H. Ren, *RSC advances*, 2020, **10**, 31881–31888.

5 K. Leung, N. B. Schorr, M. Mayer, T. N. Lambert, Y. S. Meng and K. L. Harrison, *Chemistry of Materials*, 2021, **33**, 1760–1770.

6 N. Watanabe, M. Endo and K. Ueno, *Solid State Ionics*, 1980, **1**, 501–507.

7 R. Yazami, A. Hamwi, K. Guérin, Y. Ozawa, M. Dubois, J. Giraudet and F. Masin, *Electrochemistry communications*, 2007, **9**, 1850–1855.

8 W. Liu, H. Li, J.-Y. Xie and Z.-W. Fu, *ACS Applied Materials & Interfaces*, 2014, **6**, 2209–2212.

9 W. Liu, Y. Li, B.-X. Zhan, B. Shi, R. Guo, H.-J. Pei, J.-Y. Xie and Z.-W. Fu, *The Journal of Physical Chemistry C*, 2016, **120**, 25203–25209.

10 H. Yue, W. Zhang, H. Liu, Z. Liu, G. Zhong and Y. Yang, *Nanotechnology*, 2013, **24**, 424003.

11 M. Dubois, K. Guérin, W. Zhang, Y. Ahmad, A. Hamwi, Z. Fawal, H. Kharbache and F. Masin, *Electrochimica acta*, 2012, **59**, 485–491.

12 M. Gao, D. Cai, S. Luo, Y. Yang, Y. Xie, L. Zhu and Z. Yuan, *Journal of Materials Chemistry A*, 2023.

13 B. Sayahpour, H. Hirsh, S. Bai, N. B. Schorr, T. N. Lambert, M. Mayer, W. Bao, D. Cheng, M. Zhang, K. Leung *et al.*, *Advanced Energy Materials*, 2022, **12**, 2103196.

14 N. Watanabe, R. Hagiwara, T. Nakajima, H. Touhara and K. Ueno, *Electrochimica Acta*, 1982, **27**, 1615–1619.

15 S. S. Zhang, D. Foster, J. Wolfenstine and J. Read, *Journal of Power Sources*, 2009, **187**, 233–237.

16 F. Rao, Z. Wang, B. Xu, L. Chen and C. Ouyang, *Engineering*, 2015, **1**, 243–246.

17 Y. Shao, H. Yue, R. Qiao, J. Hu, G. Zhong, S. Wu, M. J. McDonald, Z. Gong, Z. Zhu, W. Yang *et al.*, *Chemistry of Materials*, 2016, **28**, 1026–1033.

18 M. S. Whittingham, *Journal of The Electrochemical Society*, 1975, **122**, 526.

19 G. Nagasubramanian and M. Rodriguez, *Journal of power sources*, 2007, **170**, 179–184.

20 M. A. Rodriguez, M. R. Keenan and G. Nagasubramanian, *Journal of Applied Crystallography*, 2007, **40**, 1097–1104.

21 J. Read, E. Collins, B. Piekarski and S. Zhang, *Journal of The Electrochemical Society*, 2011, **158**, A504.

22 P. Giannozzi, S. Baroni, N. Bonini, M. Calandra, R. Car, C. Cavazzoni, D. Ceresoli, G. L. Chiarotti, M. Cococcioni, I. Dabo *et al.*, *Journal of physics: Condensed matter*, 2009, **21**, 395502.

23 M. J. van Setten, M. Giantomassi, E. Bousquet, M. J. Verstraete, D. R. Hamann, X. Gonze and G.-M. Rignanese, *Computer Physics Communications*, 2018, **226**, 39–54.

24 J. P. Perdew, K. Burke and M. Ernzerhof, *Physical review letters*, 1996, **77**, 3865.

25 H. J. Monkhorst and J. D. Pack, *Physical review B*, 1976, **13**, 5188.

26 O. Andreussi, I. Dabo and N. Marzari, *The Journal of chemical physics*, 2012, **136**, 064102.

27 D. Vanderbilt, *Phys. Rev. B*, 1990, **41**, 7892–7895.

28 A. Hirsch, *Nature Materials*, 2010, **9**, 868–871.

29 H. Huo, S. Radhakrishnan, L. L. Shaw and K. Nemeth, *Batteries*, 2023, **9**, 268.

30 F. J. Owens, *Solid State Communications*, 2017, **250**, 75–78.

31 P. Serafini, A. Milani, D. M. Proserpio and C. S. Casari, *J. Phys. Chem. C*, 2021, **125**, 18456—-18466.

32 A. C. Lokhande, I. A. Qattan, C. D. Lokhande and S. P. Patole, *J. Mater. Chem. A*, 2020, **8**, 918–977.

33 D. N. G. Krishna and J. Philip, *Appl. Surf. Sci. Adv.*, 2022, **12**, 100332.

34 J. M. Kahk and J. Lischner, *J. Chem. Theory Comput.*, 2023, **19**, 3276–3283.

35 S. Verdier, L. E. Ouatani, R. Dedryvère, F. Bonhomme, P. Biensan and D. Gonbeau, *Journal of The Electrochemical Society*, 2007, **154**, A1088.

36 K. Doll, J. C. Schön and M. Jansen, *The Journal of Chemical*

Physics, 2010, **133**, 024107.
37 Y.-H. Yin and W.-J. Liu, *The European Physical Journal D*, 2022, **76**, 201.

The data supporting this article have been included as part of the Supplementary Information.